Journal of
MATERIALS RESEARCH

On the design of 1-3 piezocomposites using topology optimization

O. Sigmund,[a] S. Torquato, and I. A. Aksay
Departments of Civil Engineering and Operations Research and Chemical Engineering, Princeton Materials Institute, Princeton University, Princeton, New Jersey 08544

(Received 19 March 1997; accepted 12 August 1997)

We use a topology optimization method to design 1-3 piezocomposites with optimal performance characteristics for hydrophone applications. The performance characteristics we focus on are the hydrostatic charge coefficient $d_h^{(*)}$, the hydrophone figure of merit $d_h^{(*)} g_h^{(*)}$, and the electromechanical coupling factor $k_h^{(*)}$. The piezocomposite consists of piezoelectric rods embedded in an optimal polymer matrix. We use the topology optimization method to design the optimal (porous) matrix microstructure. When we design for maximum $d_h^{(*)}$ and $d_h^{(*)} g_h^{(*)}$, the optimal transversally isotopic matrix material has negative Poisson's ratio in certain directions. When we design for maximum $k_h^{(*)}$, the optimal matrix microstructure is layered and simple to build.

I. INTRODUCTION

Piezoelectric transducers have been employed as sensors and transmitters of acoustic signals in ultrasound medical imaging, nondestructive testing, and underwater acoustics.[1,2] Besides these traditional applications, miniaturizing transducers opens up for a variety of new applications. Low-frequency transducers for underwater acoustics are known as *hydrophones.*

This paper studies a class of composite piezoelectric transducers for hydrophone applications: composites consisting of an array of parallel piezoceramic rods embedded in a polymer matrix with electrode layers in the top and bottom surfaces (see Fig. 1). Following Newnham's connectivity classification,[3] we refer to this structure as a 1-3 *composite.* The composite is poled in the longitudinal (vertical or x_3) direction. Under an incident underwater acoustic field, the composite transmits strain to the ceramic rods which is transformed into a longitudinal voltage difference and thus acts as a *sensor.* Conversely, application of an alternating current will give rise to an acoustic field by the converse piezoelectric effect.

One may ask why one would want to make a composite to begin with or, in other words, why is pure piezoceramic not used since it is the only material with piezoelectric properties? The basic problem is that under hydrostatic load, the anisotropic piezoelectric response of pure PZT is such that it has poor hydrophone performance characteristics. Specifically, consider a PZT rod poled in the axial direction (x_3-direction) subjected to hydrostatic load. The induced polarization field in the axial direction is found to be proportional to the applied pressure, i.e.,

$$D_3 = d_h^{(*)} T\,, \qquad d_h^{(*)} = d_{33}^{(*)} + 2d_{13}^{(*)}\,, \tag{1}$$

where D_3 is the dielectric displacement in the x_3-direction, T is the amplitude of the applied pressure, $d_h^{(*)}$ is the hydrostatic coupling coefficient, and $d_{33}^{(*)}$ and $d_{13}^{(*)}$ are the longitudinal and transverse piezoelectric coefficients characterizing the dielectric response for axial and lateral compression, respectively. Unfortunately, $d_{33}^{(*)}$ and $d_{13}^{(*)}$ have opposite signs, thus resulting in a relatively small hydrostatic coupling factor $d_h^{(*)}$. For instance, PZT5A has $d_{33}^{(*)} = 374pC/N$ and $d_{13}^{(*)} = 171pC/N$. Therefore, $d_h^{(*)} = 32pC/N$ which is small compared to $d_{33}^{(*)}$.

As we will see in this paper, a polymer/piezoceramic composite can have a sensitivity that is orders of magnitude greater than a pure piezoceramic device. Using a piezo/polymer composite, the factor of 2 on the transverse piezoelectric coefficient d_{13} in Eq. (1) can be lowered, or even change sign, if we use a soft matrix material or a matrix material with negative Poisson's ratio (e.g., Smith[2]), thereby ensuring a much higher hydrostatic charge coefficient.

The use of piezocomposites in hydrophone design has been studied in several papers. Hydrophones composed of piezoelectric rods in solid polymer matrices have been tested experimentally in Refs. 1, 4, and 5. Using simple models in which the elastic and electric fields were taken to be uniform in the different phases, Haun and Newnham,[3] Chan and Unsworth,[6] and Smith[2] qualitatively explained the enhancement due to Poisson's ratio effect. A more sophisticated analysis has recently been given by Avellaneda and Swart[7] using

[a]Partly on leave from Department of Solid Mechanics, Technical University of Denmark, DK-2800 Lyngby, Denmark (current and permanent address).

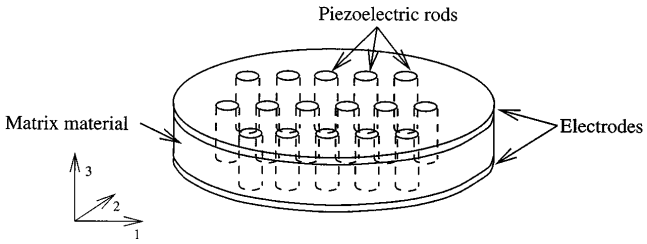

FIG. 1. Sketch of the 1-3 piezocomposite construction.

the so-called differential-effective-medium approximation. They found the effective performance factors: the hydrostatic charge coefficient d_h^*, the hydrostatic voltage coefficient g_h^*, and the electromechanical coupling factor k_h^* as functions of the effective moduli of the composite and simple structural parameters. In Ref. 7, it is assumed that the matrix material is isotropic.

Recently, Gibiansky and Torquato[8] found theoretical bounds for hydrophone design using the elastic properties of the matrix material as design variables. In contrast to Avellaneda and Swart,[7] they allowed the matrix material to be transversely isotropic. However, they did not consider finding the actual matrix microstructure corresponding to the optimal elastic properties. In this paper, we will take the first steps toward closing this gap by designing the optimal microstructural matrix topology simultaneously with the optimization of the hydrophone performance.

The design of two-dimensional material microstructures with specific or optimal elastic properties has been studied by a number of investigators. Milton and Cherkaev[9] designed two-dimensional, multi-length-scale materials, with elastic properties ranging over the entire set compatible with thermodynamics. Vigdergauz[10] and Grabovsky and Kohn[11] studied single-inclusion microstructures with extreme rigidity. Sigmund[12–14] designed material microstructures with specific elastic properties (including isotropic negative Poisson's ratio materials) using topology optimization techniques, where the microstructure is restricted to one length scale.

Less research has been devoted to the design of three-dimensional microstructures. Three-dimensional optimal rigidity materials can be made as microstructures with several length scales and the design of truss-like microstructures with extreme elastic properties as described in Sigmund.[14] However, none of these methods give practically realizable microstructures. Therefore, this paper suggests a method to design practically realizable three-dimensional microstructures using the topology optimization method and based on methods developed in aforementioned works of Sigmund.

In the proposed design procedure, the microstructural topology of the matrix material and the volume fraction of piezoelectric rods are the design variables. To find the optimal matrix topology we use the topology optimization method originally suggested by Bendøe and Kikuchi.[15] The general topology optimization procedure determines for every point in space whether there is material at that point or not. Alternatively, discretizing the design domain by finite elements, every element is either solid or void. The method has mostly been applied to two-dimensional structures, but has been extended to three dimensions in the works of Cherkaev and Palais,[16] Allaire *et al.*,[17] and Lipton and Díaz.[18]

The proposed method, for design of optimal piezocomposites, essentially follows the steps of conventional topology optimization procedures. It is an iterative procedure, each iteration implying a homogenization procedure (finite-element analysis) to determine the effective properties of the porous matrix material, an evaluation of the effective piezoelectric properties (using equations from Ref. 7), a sensitivity analysis determining the change in objective function subject to matrix microstructural change, and finally determining the optimal change in the porous matrix topology using linear programming. The procedure differs from the aforementioned general topology optimization method in three aspects. First, the design domain is the cubic base cell of a periodic material in contrast to conventional approaches which consider structures—not material microstructures. Second, the objective function is more complicated, requiring the determination of the effective matrix and piezocomposite topologies as opposed to conventional procedures that often consider relatively simple objective functions such as compliance or natural frequencies. Third, by using an "artificial material" model for intermediate element densities, we simplify the design procedure.

The paper is organized as follows: in Sec. II, we determine the effective matrix material properties as a function of the element densities. Thereafter, we determine the effective piezocomposite properties and the hydrophone coefficients as functions of the matrix properties and the volume fraction of the piezoelectric rods. In Sec. III, we briefly describe the topology optimization procedure and in Sec. IV, we consider four different design examples, namely the design of a hydrophone with maximum positive and negative hydrostatic charge coefficient $d_h^{(*)}$, maximum hydrophone figure of merit $d_h^{(*)} g_h^{(*)}$, and maximum electromechanical coupling factor $(k_h^{(*)})^2$.

II. EFFECTIVE PROPERTIES OF THE PIEZOCOMPOSITE

This section describes how the effective properties of the piezocomposites are found by a two-step procedure. First, we find the effective elastic properties of

the matrix material using a numerical homogenization method. Second, we summarize how to find the effective hydrophone properties of aforementioned matrix material with added piezoelectric rods using the approach of Avellaneda and Swart.[7]

A. Matrix properties

The design problem consists of finding the optimal microstructural topology of the matrix material which is a porous polymer. This problem can be solved using the topology optimization method, as described in the introduction. We start by discretizing the periodic base cell by a number, N, of 8-node cubic linear-displacement finite elements (using from several hundred to several thousand elements). The design procedure will determine whether each of the element should be either solid or void, allowing us to define a microstructure composed of small boxes (finite elements), as sketched in Fig. 2. To allow for the design of a detailed microstructure, the N should be at least several thousand, but even for a small number of elements, the integer-type optimization problems becomes a huge combinatorial problem which is impossible to solve. For a small design problem with $N = 100$, the number of different distributions of solid or void cubes would be astronomical ($2^{100} = 1.3 \cdot 10^{30}$). As each function evaluation requires a full finite element analysis, it is hopeless to solve the optimization problem using random search methods such as genetic algorithms or simulated annealing methods, which use a large number of function evaluations and do not make use of sensitivity information.

Following the idea of standard topology optimization procedures (and to ensure a well-posed problem), the problem is therefore relaxed by allowing the material in a given element to have intermediate densities. This makes it possible to find sensitivities with respect to design changes, which in turn allows us to use mathematical programming methods to solve the optimization problem. At the end of the optimization procedure, however, we hope to have a design where each element is either solid or void.

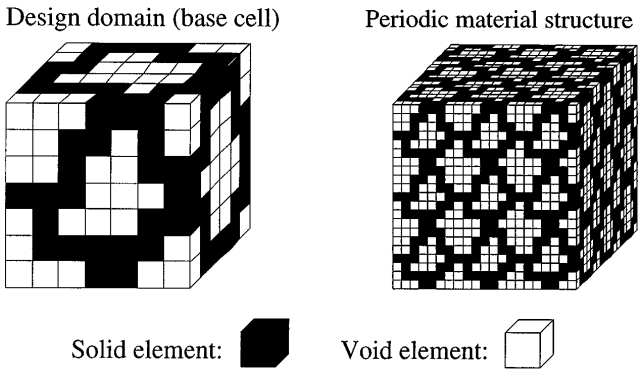

FIG. 2. Design domain and discretization for the topology optimization problem. Each cube represents one finite element, and the density of polymer material in each finite element represents a design variable.

Allowing intermediate densities, the elastic tensor C_{ij}^{e} of each element e is written as a function of the design variable x^e (element density), i.e.,

$$C_{ij}^{e} = (x^e)^{\eta} C_{ij}^{(p)}, \tag{2}$$

where $C_{ij}^{(p)}$ is the stiffness tensor of solid polymer and η is a penalty factor which ensures that the solution consists of entirely solid and "void" elements. (A material with stiffness/density relation close to the described can be realized as a tetragonal isotropic cellular microstructure.) Assuming that the base cell is discretized by N cubic finite elements, the vector of design variables x is defined as an n-vector containing the design variables. The value of each design variable is bounded to the domain $x^e \in]x_{\min}, 1\mu$, where $x_{\min}$ is a small number ($x_{\min}$ is greater than zero to ensure nonsingularity of the finite element stiffness matrix).

The effective elastic properties of the matrix material, as a function of the vector of element densities x, can be computed using numerical homogenization methods, based on finite-element calculations, as described in Bourgat[19] or Guedes and Kikuchi.[20] Assuming small strains and linear elasticity the components of the effective stiffness tensor of the matrix material, which are important for hydrophone design, can be written in matrix form as

$$C_{ij}^{(m)}(\mathbf{x}) = \begin{bmatrix} C_{11}^{(m)}(\mathbf{x}) & C_{12}^{(m)}(\mathbf{x}) & C_{13}^{(m)}(\mathbf{x}) \\ C_{12}^{(m)}(\mathbf{x}) & C_{22}^{(m)}(\mathbf{x}) & C_{23}^{(m)}(\mathbf{x}) \\ C_{13}^{(m)}(\mathbf{x}) & C_{23}^{(m)}(\mathbf{x}) & C_{33}^{(m)}(\mathbf{x}) \end{bmatrix}. \tag{3}$$

Assuming transversal isotropy, the stiffness tensor can be written in the simpler form.

$$C_{ij}^{(m)}(\mathbf{x}) = \begin{bmatrix} K^{(m)}(\mathbf{x}) & C_{13}^{(m)}(\mathbf{x}) \\ C_{13}^{(m)}(\mathbf{x}) & C_{33}^{(m)}(\mathbf{x}) \end{bmatrix}, \tag{4}$$

where the effective in-plane bulk modulus is defined as

$$K^{(m)}(\mathbf{x}) = (C_{11}^{(m)}(\mathbf{x}) + C_{12}^{(m)}(\mathbf{x}))/2. \tag{5}$$

For later use, we will define the effective in-plane shear modulus as

$$\mu^{(m)}(\mathbf{x}) = (C_{11}^{(m)}(\mathbf{x}) - C_{12}^{(m)}(\mathbf{x}))/2. \tag{6}$$

B. Properties of piezoelectric rods

The properties of the piezoelectric rods are described by the isotropic stiffness tensor $C_{ij}^{(i)}$ and the piezoelectric stress tensor $e_{ij}^{(i)}$. The transverse bulk modulus of the piezoelectric rods is given as

$$K^{(i)} = (C_{11}^{(i)} + C_{12}^{(i)})/2. \tag{7}$$

C. Constitutive relations for piezoelectric media

The constitutive relations for elastic, piezoelectric media can be written as

$$\sigma_i = C_{ij}^{(*)}\epsilon_j - e_{ik}^{(*)}E_k$$

$$D_i = e_{ij}^{(*)}\epsilon_j + \varepsilon_{ij}^{T(*)}E_j\,, \tag{8}$$

where σ_i, ϵ_j, D_i, E_j are the stress, strain, dielectric displacement, and electric field tensors and $C_{ij}^{(*)}$ and $\varepsilon_{ij}^{T(*)}$ are the effective stiffness and clamped-body permittivity tensors, respectively, and $e_{ij}^{(*)}$ is the effective piezoelectric stress matrix related to the effective piezoelectric strain matrix $d_{ij}^{(*)}$ through the relation $e_{ij}^{(*)} = C_{ik}^{(*)}d_{kj}^{(*)}$.

D. Effective hydrophone properties

The effective properties of the piezocomposite are calculated under the assumptions that (i) the length-scale associated with the microscopic variation of the matrix material is well below the diameter of the piezoelectric rods, (ii) the wavelengths of the incident acoustic field are much longer than the size of the rods, (iii) we have perfect bonding between the matrix phase and the rods, and (iv) the stiffness of the matrix material is much lower than the stiffness of the piezoelectric rods. Using these assumptions, Avellaneda and Swart[7] showed that the relevant effective parameters for hydrophone design are given as

$$\begin{aligned}
C_{13}^{(*)}(f,\mathbf{x}) &= C_{13}^{(m)}(\mathbf{x}) + fp(C_{13}^{(i)} - C_{13}^{(m)}(\mathbf{x})\\
e_{13}^{(*)}(f,\mathbf{x}) &= e_{13}^{(m)}(\mathbf{x}) + fp(e_{13}^{(i)} - e_{13}^{(m)}(\mathbf{x})\\
C_{33}^{(*)}(f,\mathbf{x}) &= C_{33}^{(m)}(\mathbf{x})\\
&\quad + f\left\{C_{33}^{(i)} - C_{33}^{(m)}(\mathbf{x}) + (p-1)\frac{(C_{13}^{(i)} - C_{13}^{(m)}(\mathbf{x}))^2}{(K^{(i)} - K^{(m)}(\mathbf{x}))}\right\}\\
e_{33}^{(*)}(f,\mathbf{x}) &= e_{33}^{(m)} + f\left\{e_{33}^{(i)} - e_{33}^{(m)}\right.\\
&\quad \left. + (p-1)\frac{(C_{13}^{(i)} - C_{13}^{(m)}(\mathbf{x}))\,(e_{13}^{(i)} - e_{13}^{(m)}(\mathbf{x}))}{(K^{(i)} - K^{(m)}(\mathbf{x}))}\right\},\\
\varepsilon_{33}^{(*)}(f,\mathbf{x}) &= \varepsilon_{33}^{(m)}\\
&\quad + f\left\{\varepsilon_{33}^{(i)} - \varepsilon_{33}^{(m)} - (p-1)\frac{(e_{13}^{(i)} - e_{13}^{(m)}(\mathbf{x}))^2}{(K^{(i)} - K^{(m)}(\mathbf{x}))}\right\},
\end{aligned} \tag{9}$$

where p is a structural parameter defined as

$$p = \frac{1}{f}\,\frac{K^{(*)}(\mathbf{x}) - K^{(m)}(\mathbf{x})}{K^{(i)} - K^{(m)}(\mathbf{x})}\,. \tag{10}$$

Following Gibiansky and Torquato,[8] the effective transverse bulk modulus $K^{(*)}(\mathbf{x})$ is taken as the lower Hashin–Shtrikman bound

$$\begin{aligned}
K^{(*)}(f,\mathbf{x}) = K^{l} &= fK^{(m)}(\mathbf{x}) + (1-f)K^{(m)}(\mathbf{x})\\
&\quad - \frac{f(1-f)\,(K^{(m)}(\mathbf{x}) - K^{(i)})^2}{fK^{(m)}(\mathbf{x}) + (1-f)K^{(i)} + \mu^{(m)}(\mathbf{x})}\,,
\end{aligned} \tag{11}$$

implying that the piezoelectric rods should be ordered in a hexagonal array to ensure optimality of the composite.

The matrix material is passive, implying the piezoelectric stress coefficients of the matrix material are zero, i.e., $e_{13}^{(m)} = e_{33}^{(m)} = 0$. We will assume that the dielectric constant $\varepsilon_{33}^{(m)}$ of the porous matrix material is equal to the dielectric constant of the polymer material. As the values of the dielectric constants of polymer and void are very small compared to the dielectric constant of the piezoelectric rods, this assumption should not change the results significantly. This was verified numerically.

For later use, we will define the matrices and vectors

$$C^{(*)} = \begin{bmatrix} K^{(*)}(f,\mathbf{x}) & C_{13}^{(*)}(f,\mathbf{x}) \\ C_{13}^{(*)}(f,\mathbf{x}) & C_{33}^{(*)}(f,\mathbf{x}) \end{bmatrix},$$

$$\mathbf{e}^{(*)} = \{e_{13}^{(*)}(\mathbf{x})\,, e_{33}^{(*)}(\mathbf{x})\}^T\,,$$

$$\mathbf{v} = \{1,1\}^T\,, \tag{12}$$

and the dilatational compliance

$$s_h^{(*)}(f,\mathbf{x}) = \mathbf{v}^T(C^{(*)})^{-1}\mathbf{v}\,. \tag{13}$$

E. Hydrophone performance

Having defined the effective hydrophone properties in the preceding subsections, we are ready to write the equations for the effective hydrophone performance coefficients.

1. The effective hydrostatic charge coefficient

$$d_h^{(*)}(f,\mathbf{x}) = d_{33}^{(*)}(f,\mathbf{x}) + 2d_{13}^{(*)}(f,\mathbf{x})\,. \tag{14}$$

2. The effective hydrostatic voltage coefficient

$$g_h^{(*)}(f,\mathbf{x}) = \frac{d_h^{(*)}(f,\mathbf{x})}{\varepsilon_{33}^{T(*)}(f,\mathbf{x})}\,. \tag{15}$$

3. A common hydrostatic figure of merit is the product

$$d_h^{(*)}(f,\mathbf{x})g_h^{(*)}(f,\mathbf{x}) = \frac{(d_h^{(*)}(f,\mathbf{x}))^2}{\varepsilon_{33}^{T(*)}(f,\mathbf{x})}\,. \tag{16}$$

4. The effective nondimensional electromechanical coupling factor

$$(k_h^{(*)})^2(f,\mathbf{x}) = \frac{(d_h^{(*)}(f,\mathbf{x}))^2}{\varepsilon_{33}^{T(*)}(f,\mathbf{x})s_h^{(*)}(f,\mathbf{x})}\,, \tag{17}$$

where the effective free body axial permittivity factor is found as $\varepsilon_{33}^{T(*)}(f,\mathbf{x}) = \varepsilon_{33}^{(*)}(f,\mathbf{x}) + \mathbf{e}^T(C^{(*)})^{-1}\mathbf{e}$. We choose to work with the squared electromechanical coupling factor since this has a physical meaning of electric output divided by dilatational compliance.

Using previous definitions, $d_h^{(*)}$, $d_h^{(*)}g_h^{(*)}$, and $(k_h^{(*)})^2$ can be rewritten in the following way

$$
\begin{aligned}
&d_h^{(*)}(f,\mathbf{x}) = \mathbf{v}^T(C^{(*)})^{-1}\mathbf{e}^{(*)}\,,\\
&d_h^{(*)}(f,\mathbf{x})g_h^{(*)}(f,\mathbf{x}) = \frac{(\mathbf{v}^T(C^{(*)})^{-1}\mathbf{e}^{(*)})^2}{\varepsilon_{33}^{(*)}(f,\mathbf{x}) + (\mathbf{e}^{(*)})^T(C^{(*)})^{-1}\mathbf{e}^{(*)}}\,,\\
&(k_h^{(*)}(f,\mathbf{x}))^2\\
&\qquad = \frac{(\mathbf{v}(C^{(*)})^{-1}\mathbf{e}^{(*)})^2}{\varepsilon_{33}^{(*)}(f,\mathbf{x}) + (\mathbf{e}^{(*)})^T(C^{(*)})^{-1}\mathbf{e}^{(*)})\mathbf{v}(C^{(*)})^{-1}\mathbf{e}^{(*)}\mathbf{v}}\,.
\end{aligned}
\tag{18}
$$

With Eqs. (18) we have defined the important performance criteria for hydrophone design as a function of element densities $\mathbf{x}$ of the discretized base cell modeling the matrix material, and as a function of the volume reaction of piezoelectric rods f embedded in the matrix.

III. OPTIMIZATION

In the preceding section, we have found the piezoelectric performance coefficients in terms of the matrix microstructural design variables $\mathbf{x}$ (the element densities) and the volume fraction of the piezoelectric rods f.

Now, we can consider the following optimization problem:

$$
\begin{aligned}
&\textit{Maximize}\text{: } |d_h^{(*)}|,\ d_h^{(*)}g_h^{(*)} \text{ or } (k_h^{(*)})^2\\
&\textit{Variables}\text{: Volume fraction } f \text{ and element densities } \mathbf{x}\\
&\textit{Subject to}\text{: Transversal isotropy of the matrix material}\\
&\qquad \textit{and}\text{: Lower bound constraint on bulk modulus}\\
&\qquad\qquad \text{of the matrix } K^{(m)}\\
&\qquad \textit{and}\text{: Lower bound constraint on the volume}\\
&\qquad\qquad \text{fraction of piezorods } f\,.
\end{aligned}
\tag{19}
$$

The previous analysis assumes that the matrix material is transversally isotropic. Specifying horizontal, and two vertical symmetry planes in the base cell ensures orthotropy of the matrix material. To ensure transversal isotropy, two additional criteria must be fulfilled, namely that $C_{11}^{(m)} = C_{22}^{(m)}$ and that $C_{13}^{(m)} = C_{23}^{(m)}$. The transversal isotropy requirements to the matrix is implemented as a penalty term added to the cost function. The normalized error in obtaining transversal transversal isotropy of the matrix material can thus be written as

$$
Error_{\text{tr.iso}}(\mathbf{x}) = \frac{(C_{11}^{(m)}(\mathbf{x}) - C_{22}^{(m)}(\mathbf{x}))^2 + (C_{13}^{(m)}(\mathbf{x}) - C_{23}^{(m)}(\mathbf{x}))^2}{(K^{(m)}(\mathbf{x}))^2}\,.
\tag{20}
$$

For some of the design examples, the in-plane bulk modulus $K^{(m)}$ approached zero when we tried to maximize the hydrophone performance. This would result in an impractical (very soft) design; hence, we introduce the lower bound constraint on the in-plane bulk modulus.

The optimization problem can now be formalized as

$$
\begin{aligned}
&\textit{Minimize}\text{: } \Phi(f,\mathbf{x}) = F(f,\mathbf{x}) + rError_{\text{tr.iso.}}(\mathbf{x})\\
&\textit{Subject to}\text{: } K_{\min}^{(m)} \leqslant K^{(m)}(\mathbf{x})\\
&\qquad \textit{and}\text{: } f_{\min} \leqslant f\,,\\
&\qquad \textit{and}\text{: } 0 < \mathbf{x}_{\min} \leqslant \mathbf{x} \leqslant 1\,,
\end{aligned}
\tag{21}
$$

where the objective function F is one of the performance criteria given in Eqs. (18), and $\Phi(f,\mathbf{x})$ is the global objective function. The minimum value of the element densities is $x_{\min} = 10^{-4}$, not zero to prevent the stiffness matrix in becoming singular.

A. Sequential linear programming method

The optimization problem, Eqs. (21), is nonlinear, and must be solved iteratively. To solve it, we will use a mathematical programming method called sequential linear programming (SLP), which consists in the sequential solving of an approximate linear subproblem, obtained by writing linear Taylor series expansions for the objective and constraint functions. The SLP method was successfully used in optimization of truss structures by Pederson[21] and was evaluated as a robust, efficient, and easy to use optimization algorithm in a review paper by Schittkowski[22] and is used for solving large-scale topology optimization problems with multiple constraints in Sigmund and Torquato.[23]

The optimal volume fraction of piezoelectric rods f is found by a golden sectioning method in each iteration step. Having found the optimal f, the optimization problem, Eqs. (21), is linearized around the current design point $\mathbf{x}$ using the first part of a Taylor series expansion, and the vector of optimal design changes $\Delta\mathbf{x}$ is found by solving the linear programming problem

$$
\begin{aligned}
&\textit{Minimize}\text{: } \Phi + \left\{\frac{\partial\Phi}{\partial\mathbf{x}}\right\}^T\{\Delta\mathbf{x}\},\\
&\textit{Subject to}\text{: } K_{\min}^{(m)} - K^{(m)}(\mathbf{x}) \leqslant \left\{\frac{\partial K^{(m)}(\mathbf{x})}{\partial\mathbf{x}}\right\}^T\Delta\mathbf{x}\,,\\
&\qquad\qquad : \Delta\mathbf{x}_L \leqslant \Delta\mathbf{x} \leqslant \Delta\mathbf{x}_U\,,
\end{aligned}
\tag{22}
$$

where $\Delta \mathbf{x}_L$ and $\Delta \mathbf{x}_U$ are move-limits on the design variables. The move-limits are adjusted for the absolute limits given in Eqs. (21).

The applied move-limit strategy is important for the stable convergence of the algorithm. Here we use the simple rule that the move-limit for a specific design variable is increased by a factor of 1.4, if the change in the design variable has the same sign for two subsequent steps. Similarly the move-limit is decreased by a factor of 0.6, if the change in the design variable has opposite signs for two subsequent steps.

To solve the linearized subproblem, Eq. (22), we need to find the sensitivities of the hydrostatic performance coefficients and of the in-plane matrix bulk modulus with respect to change in design variable x^e namely,

$$\frac{\partial d_b^{(*)}}{\partial x^e}, \qquad \frac{\partial [d_h^{(*)} g_h^{(*)}]}{\partial x^e}, \qquad \frac{\partial [(k_h^{(*)})^2]}{\partial x^e},$$

and

$$\frac{\partial K^{(m)}}{\partial x^e}.$$

The sensitivities are derived analytically as functions of the matrix constitutive tensor $C^{(m)}$ and the sensitivities $\partial C^{(m)}/\partial x^e$.

The sensitivities $\partial C^{(m)}/\partial x^e$ can be found directly from the strain fields already computed by the homogenization procedure and are calculated locally for each element (e.g., Sigmund and Torquato[23]). This means that no additional finite-element problems have to be solved to find the sensitivities needed.

B. Design procedure

The design procedure consists of the following steps:

1. Take a (porous) matrix material, described by a cubic base cell, discretized by finite elements;
2. Find the effective matrix properties $C_{ij}^{(m)}$ as a function of the element densities $\mathbf{x}$ using the numerical homogenization method and finite-element analysis;
3. Find the effective piezocomposite properties as functions of the element densities $\mathbf{x}$ and the volume fraction of piezo electric rods f [Eqs. (9)];
4. Find the hydrophone performance coefficients [Eqs. (18)];
5. Find optimal f by performing golden sectioning loop over steps 3, 4, and 5 until convergence;
6. Perform sensitivity analysis (with respect to density change of each finite element);
7. Change matrix topology (element densities) using linear programming;
8. Go to step 2 (repeat until convergence).

The whole procedure is implemented in FORTRAN code. To solve the finite element problems connected with the numerical homogenization procedure, we use an Element-By-Element Preconditioned Conjugate Gradient (EBE-PCG) method. The PCG solver is described in Numerical Recipes[24] and its application to finite element problems is discussed in Hollister and Riemer,[25] who use the method for the microstructural analysis of human bone structure discretized by up to one million finite elements. The big advantage of the EBE-PCG solver, in connection with the current design problem, is, that only one element stiffness matrix must be stored. Assembly and inversion of the (huge) global stiffness matrix associated with the finite element problems is circumvented.

The linear programming problem Eqs. (22) is solved using the linear programming code DSPLP[26] from the SLATEC Library.

Applying the topology optimization method, as described, often results in "optimal solutions" with regions of alternating solid and void elements, referred to as checkerboards. The regions are seen in many works on general topology optimization, and it was earlier believed that such regions represented optimal microstructure on the finite-element level. However, two recent papers by Jog and Haber[27] and Díaz and Sigmund[28] conclude that regions with checkerboard patterns have artificially high (numerical) stiffness (higher than the theoretical bounds) and can be explained by poor numerical modeling of the stiffness of checkerboards by lower order finite elements.

Another problem, due to the finite-element discretization, is mesh-dependency, which refers to the nonconvergence of solutions with mesh-refinement. Refining the finite-element mesh should ideally result in the same topology as for a coarse mesh but with better definitions of the boundaries between the material phases. To avoid the checkerboard and mesh-dependency problems, we use a filtering method, where the density updates are based on low-pass filtered strain energy fields as suggested in Sigmund.[12,29]

IV. DESIGN EXAMPLES

In this section, we apply the proposed procedure to the design of four different piezo composites with maximum $d_h^{(*)}$, minimum (maximum negative) $d_h^{(*)}$, maximum $d_h^{(*)} g_h^{(*)}$, and maximum $(k_h^{(*)})^2$, respectively. The base cell is discretized with 16 by 16 by 16 (=4096) cubic finite element. By variable linking due to symmetry, the number of design variables (element densities) can be decreased to $4096/8 = 512$.

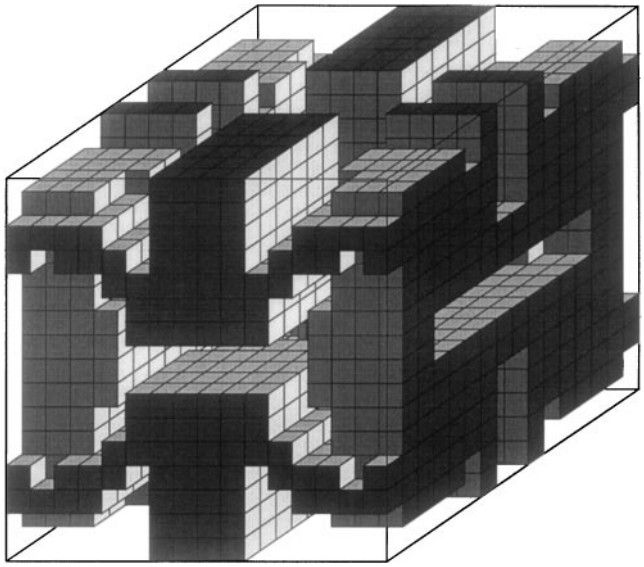

FIG. 3. Example "a": Optimal microstructure (one unit cell) for maximization of the piezoelectric charge coefficient $d_h^{(*)}$.

A. Properties of the piezoceramic and polymer

The actual properties of the PZT-ceramic rods are taken as

$$C^{(i)} = \begin{bmatrix} 120 & 75 & 75 \\ 75 & 120 & 75 \\ 75 & 75 & 111 \end{bmatrix} \cdot 10^9 \text{ Pa},$$

$$e_{13}^{(i)} = -5.4 \text{ C/m}^2, \quad e_{33}^{(i)} = 15.8 \text{ C/m}^2,$$

$$\varepsilon_{33}^{T(i)} = 827\varepsilon_0. \tag{23}$$

Young's modulus of a typical amorphous polymer material is $2.5 \cdot 10^9$ Pa and Poisson's ratio is 0.37, which give the following values of the polymer stiffness tensor:

$$C^{(p)} = \begin{bmatrix} 4.4 & 2.6 & 2.6 \\ 2.6 & 4.4 & 2.6 \\ 2.6 & 2.6 & 4.4 \end{bmatrix} \cdot 10^9 \text{ Pa},$$

$$e_{13}^{(p)} = e_{33}^{(p)} = 0, \quad e_{33}^{T(p)} = 13.5\epsilon_0. \tag{24}$$

The value of the dielectric constant in vacuum is

$$\varepsilon_0 = \frac{1}{4\pi} \frac{10^{-9}}{8.98755} \frac{C^2}{Nm^2}. \tag{25}$$

The minimum value of the in-plane bulk modulus of the matrix material is chosen as 3% of solid polymer, i.e., $K_{\min} = 0.11 \cdot 10^9$ Pa and the minimum volume fraction of the piezorods is $f_{\min} = 0.01$.

We consider the four design examples: (a) maximization of $d_h^{(*)}$, (b) minimization of $d_h^{(*)}$, (c) maximization of $d_h^{(*)} g_h^{(*)}$, and (d) maximization of $(k_h^{(*)})^2$. The resulting microstructure topologies are shown in Figs. 3, 5, 6, and 7, and the resulting hydrophone properties are shown in Table I. In the following sections we will discuss the individual examples and the mechanisms behind the enhanced properties.

B. Example a: Maximization of $d_h^{(*)}$

The resulting optimal microstructure for maximization of the hydrostatic charge coefficient $d_h^{(*)}$ is seen in Fig. 3.

The resulting effective properties of the matrix material are

$$C^{(m)} = \begin{bmatrix} 0.246 & 0.018 & -0.072 \\ 0.018 & 0.246 & 0.072 \\ -0.072 & -0.072 & 0.216 \end{bmatrix} \cdot 10^9 \text{ Pa}, \tag{26}$$

or $\nu_{12}^{(m)} = \nu_{21}^{(m)} = -0.027$, $\nu_{13}^{(m)} = -0.27$, $\nu_{31}^{(m)} = -0.34$, and the horizontal and vertical Young's moduli $E_1^{(m)} = 0.23 \cdot 10^9$ Pa $E_3^{(m)} = 0.18 \cdot 10^9$ Pa, respectively. We note that the vertical Poisson's ratio is negative, which means that horizontal forces are inverted and act like compressive forces in the vertical direction and result in the enhancement of the hydrostatic charge coefficient. This means that the negative Poisson's ratio of the matrix material makes the effective $d_{13}^{(*)}$-coefficient positive, thus enhancing the overall hydrostatic behavior.

The negative Poisson's ratio behavior of the microstructure in Fig. 3 can be difficult to imagine. To visualize the mechanism behind the negative Poisson's ratio behavior, we show a two-dimensional interpretation in Fig. 4. Seen from the front (1-3 plane), the negative Poisson's ratio behavior is seen to resemble the mechanism behind the inverted honeycomb structure.[30,31] Seen from the side (2-3 plane), the mechanism is seen to be slightly different. Note that the material structure does not need

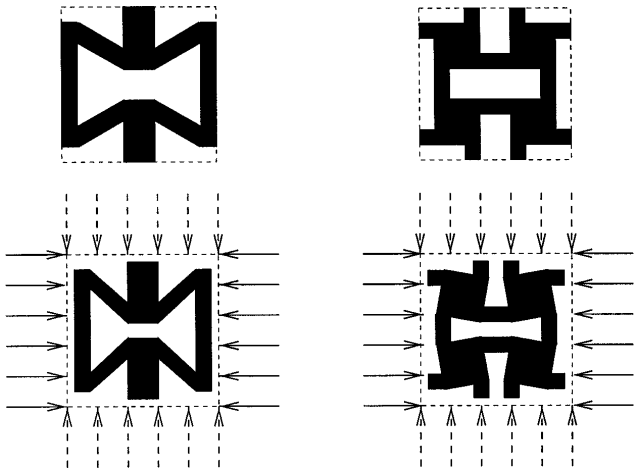

FIG. 4. Schematic representation of an equivalent two-dimensional composite that yields the (vertical) negative Poisson's ratio behavior of example "a" (Fig. 5). Left: front (1-3 plane) view, Right: side (2-3 plane) view. When the microstructures are compressed horizontally (solid arrows), they contract vertically (dashed arrows).

to be hexagonal or fully symmetric to be transversally isotropic (see, for example, Ref. 32 or Ref. 23).

C. Example b: Minimization of $d_h^{(*)}$

The resulting optimal microstructure for minimization of the effective piezoelectric charge coefficient $d_h^{(*)}$ is seen in Fig. 5.

The resulting effective properties of the matrix material are

$$C^{(m)} = \begin{bmatrix} 0.228 & 0.036 & 0.235 \\ 0.036 & 0.228 & 0.235 \\ 0.235 & 0.235 & 0.994 \end{bmatrix} \cdot 10^9 \text{ Pa}, \qquad (27)$$

or $\nu_{12}^{(m)} = \nu_{21}^{(m)} = -0.11$, $\nu_{13}^{(m)} = 0.89$, $\nu_{31}^{(m)} = 0.26$, $E_1^{(m)} = 0.17 \cdot 10^9$ Pa, and $E_3^{(m)} = 0.58 \cdot 10^9$ Pa. We see that the vertical Poisson's ratio is high ($\nu_{13}^{(m)} = 0.89$), which means that the microstructure tries to enhance the $d_{13}^{(*)}$ factor (making it more negative), resulting in a high negative value of the overall hydrostatic charge coefficient $d_h^{(*)}$.

D. Example c: Maximization of $d_h^{(*)} g_h^{(*)}$

The resulting optimal microstructure for maximization of the hydrophone figure of merit $d_h^{(*)} g_h^{(*)}$ is seen in Fig. 6.

$$C^{(m)} = \begin{bmatrix} 0.232 & 0.032 & -0.070 \\ 0.032 & 0.232 & -0.070 \\ -0.070 & -0.070 & 0.146 \end{bmatrix} \cdot 10^9 \text{ Pa}, \qquad (28)$$

or $\nu_{12}^{(m)} = \nu_{21}^{(m)} = 0.09$, $\nu_{13}^{(m)} = -0.27$, $\nu_{31}^{(m)} = -0.48$, $E_1^{(m)} = 0.20 \cdot 10^9$ Pa, and $E_{33}^{(m)} = 0.11 \cdot 10^9$ Pa.

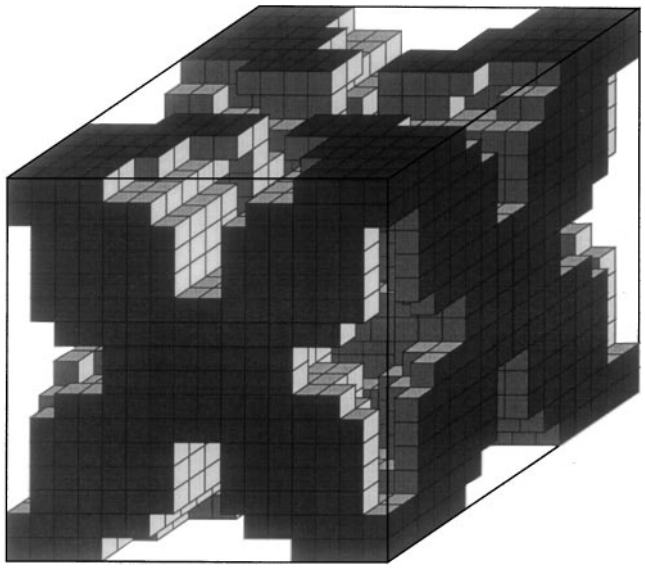

FIG. 5. Example "b": Optimal microstructure (one unit cell) for minimization of the effective piezoelectric charge coefficient $d_h^{(*)}$.

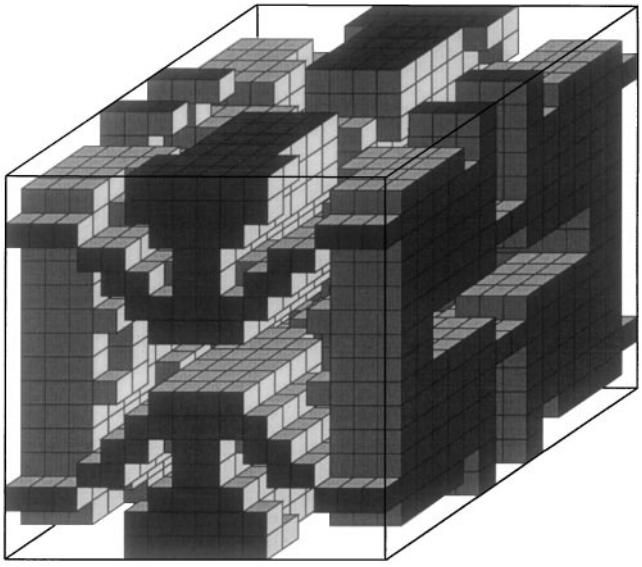

FIG. 6. Example "c": Optimal microstructure (one unit cell) for maximization of the hydrophone figure of merit $d_h^{(*)} g_h^{(*)}$.

The microstructure for this example resembles the microstructure obtained for maximization of d_h^* in example "a" (Fig. 3). The only difference is that the optimization procedure turns out a design with as much void as possible in order to minimize the effective dielectric constant $\varepsilon_{33}^{T(*)}$, in turn leading to maximum hydrostatic figure of merit $d_h^{(*)} g_h^{(*)}$ [see Eq. (16)]. As seen in Table I, the dilatational compliance for this design is high, which means that the final design is soft and impractical.

E. Example d: Maximization of $(k_h^{(*)})^2$

The resulting optimal microstructure for maximization of the effective electromechanical coupling factor $(k_h^{(*)})^2$ is seen in Fig. 7 and an interpretation is seen in Fig. 8.

The optimal matrix properties for this example are

$$C^{(m)} = \begin{bmatrix} 2.31 & 0.86 & 1.01 \\ 0.86 & 2.31 & 0.01 \\ 0.01 & 0.01 & 0.02 \end{bmatrix} \cdot 10^9 \ N/m^2, \qquad (29)$$

or $\nu_{12}^{(m)} = \nu_{21}^{(m)} = 0.37$, $\nu_{13}^{(m)} = 0.003$, $\nu_{31}^{(m)} = 0.32$, $E_1^{(m)} = 2.0 \cdot 10^9$ Pa, and $E_3^{(m)} = 0.02$ Pa.

From Fig. 8, we see that the optimal hydrophone composition is a layered structure of matrix material with embedded piezoelectric rods. The explanation for this is that the optimization procedure tries to decouple the horizontal forces working on $d_{13}^{(*)}$, leading to an overall piezoelectric charge coefficient nearly equal to $d_{33}^{(*)}$. The hydrostatic charge coefficient does not become exactly equal to $d_{33}^{(*)}$ since there is a tradeoff in obtaining

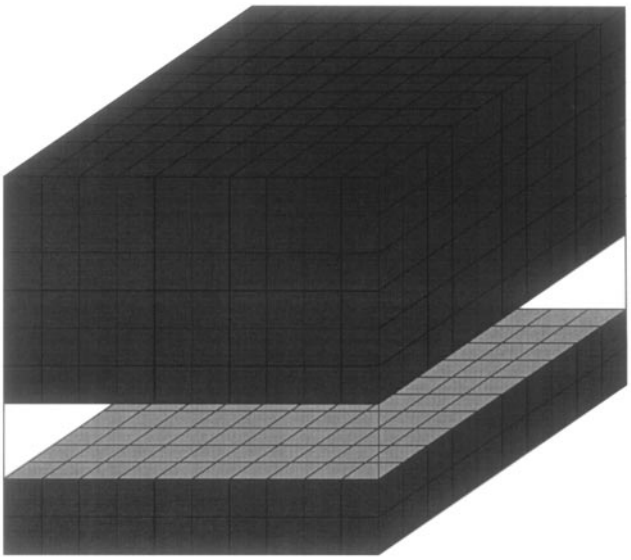

FIG. 7. Example "d": Optimal microstructure (one unit cell) for maximization of the effective electromechanical coupling factor $(k_h^{(*)})^2$.

low dilatational compliance and low dielectric constant [see Eq. (17)]. Note that the number of layers sketched in Fig. 8 is picked arbitrarily. The microstructure is determined under the assumption that the length scale of the matrix structure is much smaller than the length scale of the piezoelectric rods. Experiments and manufacturability constraints will determine the actual number and thickness of layers in the final hydrophone design.

V. MANUFACTURING

Various options exist for the fabrication of our optimal three-dimensional microstructures. Our approach is based on a stereolithography method developed by 3-D Systems, Inc.[33] In this method, a laser beam is focused onto a photocurable solution or a dispersion to induce photocuring of an agent in the continuous liquid phase. A desired object is built layer by layer by spreading a thin film with layer thicknesses between 50 and 200 μm, and then laser-curing the film to define a pattern. The layering is repeated multiple times until a desired three-dimensional body is completed (Fig. 9). The two-dimensional sections are created from a three-dimensional solid AutoCAD file, and the motion of the laser beam to cure the two-dimensional section is controlled by a computer interpreting the CAD file. Although this method was first developed to fabricate polymeric prototypes, it has now been extended to ceramics with the use of highly concentrated colloidal suspensions.[34,35] A quantitative model of light propagation in the ceramic dispersion has been developed to predict curing depths, to calculate lateral light dispersion which will cause broadening of cured lines, and to determine the spatial profile of photon intensity to program laser writing beam speeds required for curing.[35] We believe this approach will be ideal for testing out the optimal models produced by the formalism established in this paper. A prototype[36] consisting of one base cell in larger scale (8 mm cubed) for the design in which $d_h^{(*)}$ is maximized (see Fig. 3) is shown in Fig. 9. The base cell was produced by the above-mentioned manufacturing technique.

Two-dimensional microstructures with negative Poisson's ratios have also been manufactured in microscale (base cell size 50 μm) at Mikroelektronik Centret, Denmark Technical University (see Larsen, Sigmund, and Bouwstra[37]).

VI. CONCLUSIONS

This paper has shown how hydrophone performance can be increased by orders of magnitude by use of

TABLE I. Effective values for pure piezoceramic, optimal piezocomposite with solid matrix and optimal piezocomposite with topology-designed matrix.

Ex. ν	Objective	f	$d_{13}^{(*)}$ pC/N	$d_{33}^{(*)}$ pC/N	$d_h^{(*)}$ pC/N	$d_h^{(*)} g_h^{(*)}$ p (Pa)$^{-1}$	$(k_h^{(*)})^2$	$s_h^{(*)}$ n (Pa)$^{-1}$
Pure ceramic								
		1.0	−171	374	32	0.068	0.0061	0.011
Solid matrix with rods								
	Max. $d_h^{(*)}$	0.211	−125	318	68	1.50	0.0065	0.22
	Max. $d_h^{(*)} g_h^{(*)}$	0.036	− 63	167	41	3.89	0.0134	0.29
	Max. $(k_h^{(*)})^2$	0.041	− 67	167	41	3.87	0.0135	0.29
Optimal matrix with rods								
a	Max. $d_h^{(*)}$	0.042	75	346	497	399	0.049	7.9
b	Min. $d_h^{(*)}$	0.069	−272	326	−219	48	0.007	6.8
c	Max. $d_h^{(*)}$	0.010	78	310	465	1286	0.117	11
d	Max. $(k_h^{(*)})^2$	0.010	− 4	356	348	685	0.292	2.3

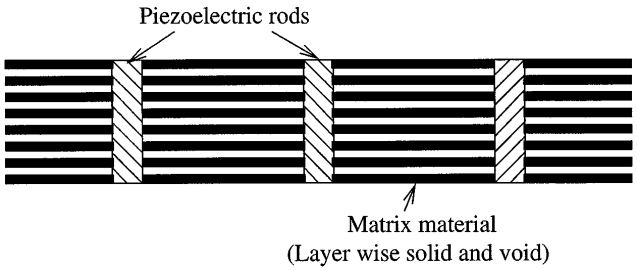

FIG. 8. Interpretation (vertical cut) of the piezo-composite design for maximization of $(k_h^{(*)})^2$.

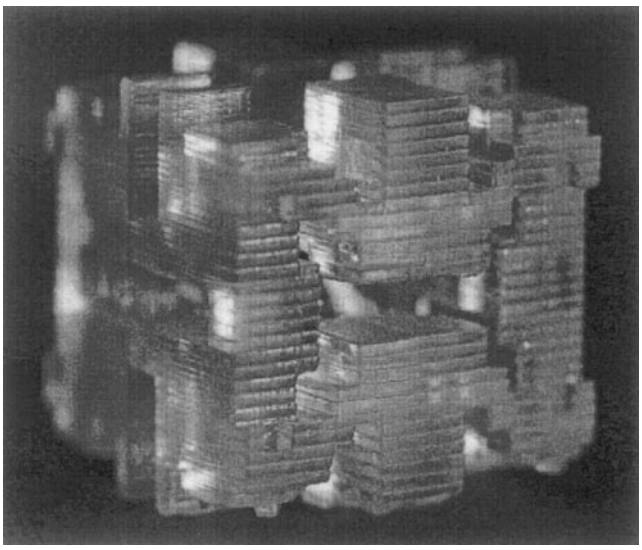

FIG. 9. Prototype of one base cell made by stereolithography.[36]

topology optimization methods for the design of polymer matrix material with piezoelectric rod inclusions.

Our goal was to design hydrophones for maximum and minimum hydrostatic charge coefficient $d_h^{(*)}$, maximum hydrophone figure of merit $d_h^{(*)} g_h^{(*)}$, and maximum electromechanical coupling factor $k_h^{(*)}$. The resulting device for *minimum* hydrostatic charge coefficient (example "b") has a lower absolute value compared to the device for *maximum* hydrostatic charge coefficient (example "a") and is therefore discarded The resulting device for maximum $d_h^{(*)} g_h^{(*)}$ (example "c") has a high dilatational compliance and is discarded since it would be too deformable under moderate loads.

Comparing the performance of examples "a" and "d" [maximum $d_h^{(*)}$ and maximum $(k_h^{(*)})^2$, respectively], the best device is probably example "d" since it is good for all performance criteria; i.e., it has a low dilatational compliance (important for high pressure underwater applications), and it is very simple to build in practice. Design example "d" enhances the values $d_h^{(*)}$, $d_h^{(*)} g_h^{(*)}$, and $(k_h^{(*)})^2$ over pure piezoceramics by factors of 11, 10,000, and 7, respectively. Comparing the performance of example "d" with the performance of the optimal composite of piezo rods and solid polymer shows improvement factors of 5, 180, and 25, respectively.

The suggested hydrophone devices have, so far, not been built in practice. We expect that imperfect interface bonding, packaging, and other practical problems will degrade the overall performance of the hydrophone designs suggested here. Nevertheless, the suggested microstructures can provide guidance for further developments of hydrophone design.

We considered fixed topology of the rods (vertical rods). The next step will be to let the shape of the rods to be free to vary as well. This can be done using the three-phase topology method developed in Sigmund and Torquato.[23,38]

ACKNOWLEDGMENTS

The authors express their gratitude to L. Gibiansky, M. P. Bendsøe, and P. Pedersen for helpful discussions. R. Garg's help in producing prototype cells (which will be described elsewhere[36]) is also gratefully acknowledged. This work received support from the ARO/MURI Grant DAAH04-95-1-0102 (OS, ST, and IA) and from Denmark's Technical Research Council (Programme of Research on Computer-Aided Design) (OS).

REFERENCES

1. R. E. Newnham and G. R. Ruchau, J. Am. Ceram. Soc. **74**, 463 (1991).
2. W. A. Smith, in *Proceedings of IEEE Ultrasonics symposium* (IEEE, 1991).
3. R. E. Newnham, Ferroelectrics **68**, 1 (1986).
4. K. A. Klicker, J. V. Biggers, and R. E. Newnham, J. Am. Ceram. Soc. **64**, 5 (1991).
5. R. Y. Ting, A. A. Shaulov, and W. A. Smith, Ferroelectrics **132**, 69 (1992).
6. H. L. W. Chan and J. Unsworth, IEEE, Trans. Ultrasonic Ferroelectrics in Frequency Control **36**, 434 (1989).
7. M. Avellaneda and P. J. Swart, unpublished.
8. L. V. Gibiansky and S. Torquato, J. Mech. Phys. Solids (in press, 1997).
9. G. W. Milton and A. V. Cherkaev, J. Eng. Mater. Technol., Trans. ASME **117**, 483 (1995).
10. S. B. Vigdergauz, Mech. Solids **24**, 57 (1989).
11. Y. Grabovsky and R. V. Kohn, J. Mech. Phys. Solids **43**, 949 (1995).
12. O. Sigmund, Ph.D. Thesis, Department of Solid Mechanics, Technical University of Denmark, 1994).
13. O. Sigmund, Int. J. Solids Struct. **31**, 2313 (1994).
14. O. Sigmund, Mech. Mater. **20**, 351 (1995).
15. M. P. Bendsøe and N. Kikuchi, Comput. Methods in Appl. Mech. Eng. **71**, 197 (1988).
16. A. Cherkaev and R. Palais, unpublished.
17. G. Allaire, E. Bonnetier, G. Francfort, and F. Jouve, unpublished.
18. R. Lipton and A. R. Díaz, in *First World Congress on Structural and Multidisciplinary Optimization*, edited by G. I. N. Rozvany and Olhoff (N. Pergamon, Goslar, Germany, 1995), pp. 161–168.
19. J. F. Bourgat, *Lecture Notes in Mathematics* (Springer-Verlag, Berlin, 1997), pp. 330–356.

20. J. M. Guedes and N. Kikuchi, Computer Methods Appl. Mech. Eng. **83**, 143 (1991).
21. P. Pedersen, in *AGARD Conference Proceedings No. 36, Symposium on Structural Optimization* (1970), pp. 189–192.
22. K. Schittkowski, Struct. Optimization **7**, 1 (1994).
23. O. Sigmund and S. Torquato, J. Mech. Phys. Solids **45**, 1037 (1997).
24. W. H. Press, S. A. Teukolsky, W. T. Vetterling, and B. P. Flannery, *Numerical Recipes in Fortran* (Cambridge University Press, England, 1992).
25. S. R. Hollister and B. A. Riemer, in *SPIE, volume 2035, Mathematical Methods in Medical Imaging II* (1993), pp. 95–106.
26. R. J. Hanson and K. L. Hiebert, Technical Report No. SAND81-0297, Sandia National Laboratories (unpublished).
27. C. S. Jog and R. B. Haber, Computer Methods Appl. Mech. Eng. **130**, 203 (1996).
28. A. R. Díaz and O. Sigmund, Struct. Optimization **10**, 40 (1995).
29. O. Sigmund, Mech. Struct. Machines **25**, 495 (1997).
30. R. F. Almgren, J. Elast. **12**, 839 (1985).
31. A. G. Kolpakov, PMM J. Appl. Math. Mech., U.S.S.R. **49**, 739 (1985).
32. O. Sigmund, in *Proceedings of the Third International Conference on Intelligent Material*, ICIM96, Lyon, June, edited by P. Gobin (SPIE vol. 2779, 1996).
33. P. Jacobs, *Rapid Prototyping and Manufacturing–Fundamentals of Stereolithography* (SME, Dearborn, MI, 1992).
34. M. L. Griffith and J. W. Halloran, J. Am. Ceram. Soc. **79**, 2601 (1996).
35. R. Garg, R. K. Prud'homme, I. A. Aksay, F. Liu, and R. Alfano, J. Opt. Soc. Am. (in press).
36. R. Garg *et al.*, unpublished.
37. U. D. Larsen, O. Sigmund, and S. Bouwstra, J. Microelectromechanical Systems, **6**, 99 (1997).
38. O. Sigmund and S. Torquato, Appl. Phys. Lett. **69**, 3203 (1996).